LANGMUIR

pubs.acs.org/Langmuir Article

Intercalation of CO_2 Selected by Type of Interlayer Cation in Dried Synthetic Hectorite

Kristoffer W. Bø Hunvik,* Konstanse Kvalem Seljelid, Dirk Wallacher, Alexsandro Kirch, Leide P. Cavalcanti, Patrick Loch, Paul Monceyron Røren, Paulo Henrique Michels-Brito, Roosevelt Droppa-Jr, Kenneth Dahl Knudsen, Caetano Rodrigues Miranda, Josef Breu, and Jon Otto Fossum*

Cite This: *Langmuir* 2023, 39, 4895−4903

Read Online

ACCESS | Metrics & More | Article Recommendations

ABSTRACT: Clay minerals are abundant in caprock formations for anthropogenic storage sites for CO_2, and they are potential capture materials for CO_2 postcombustion sequestration. We investigate the response to CO_2 exposure of dried fluorohectorite clay intercalated with Li^+, Na^+, Cs^+, Ca^{2+}, and Ba^{2+}. By *in situ* powder X-ray diffraction, we demonstrate that fluorohectorite with Na^+, Cs^+, Ca^{2+}, or Ba^{2+} does not swell in response to CO_2 and that Li-fluorohectorite does swell. A linear uptake response is observed for Li-fluorohectorite by gravimetric adsorption, and we relate the adsorption to tightly bound residual water, which exposes adsorption sites within the interlayer. The experimental results are supported by DFT calculations.

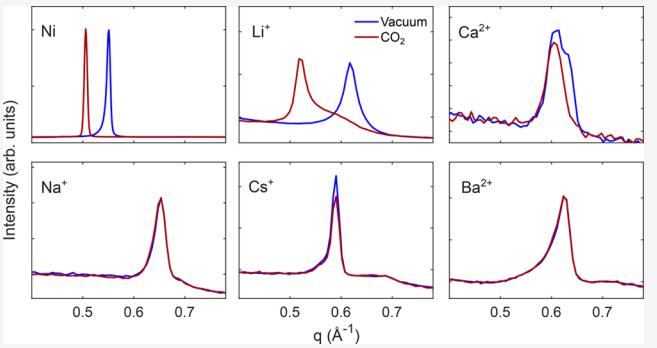

INTRODUCTION

Understanding how carbon dioxide may adsorb in the interlayers of clay minerals and tuning these mechanisms could result in pathways for mitigating greenhouse gas emissions. Smectite clays both adsorb CO_2[1−14] and are present in caprock formations for the storage of anthropogenic CO_2;[15] however, the full mechanisms for CO_2 adsorption in these materials are still unresolved.

Smectites are nanolayered phyllosilicates that consist of two tetrahedral sheets sandwiching an octahedral sheet, where isomorphic substitutions in these sheets lead to a negative layer charge that is compensated for by interlayer cations. These interlayer cations are readily hydrated, depending on the type of cation, and swelling in response to humidity occurs.[16−18] In addition, CO_2 may intercalate and result in crystalline swelling.[3,5,8,11,19,20]

The swelling response to CO_2 for smectites has received considerable attention in the literature. The swelling of hydrated clays and swelling in response to wet-supercritical CO_2 have shown that a small amount of humidity enhances the CO_2 adsorption; however, at high relative humidities, the CO_2 is displaced by water, as the solvation energy is higher for water than for CO_2.[21−28]

When the clay is dehydrated, open questions remain. For Wyoming montmorillonite (SWy-2) exchanged with Na^+, NH_4^+ and Cs^+ swelling is observed only for the larger cations under dry supercritical CO_2 exposure.[11] In ref 29, where hectorite with a mix of F^- and OH^- substitutions is studied, swelling is observed with Cs^+ as the interlayer cation, not for the smaller cation Na^+. From simulations on OH-hectorite,[29] it is argued that smaller cations such as Li^+, Na^+, Mg^{2+}, and Ca^{2+} have a global energy minimum in the collapsed zero water layer state (0WL). For larger cations such as K^+, Rb^+, Cs^+, Sr^{2+}, and Ba^{2+}, a global energy minimum is found for the monolayer state (1WL), and the clay with these cations will spontaneously intercalate CO_2. On the other hand, for dried synthetic fluorohectorite (Hec) it has been reported that with Li^+ and Na^+ as the interlayer cations the clay swells in response to CO_2;[3,4] however, for Na-Hec it was later shown that this is not always the case.[30] It is argued that the mechanism behind this is that the interlayer is "propped open" by the cation size and thus the interlayer spacing is sufficiently large for adsorption.[11,20] Cations with a size comparable to a CO_2 monolayer, in particular, Cs^+ and tetramethylammonium (TMA^+), have been shown for anhydrous montmorillonite (SWy-2) to provide an optimum cation size for the highest CO_2

Received: November 13, 2022
Revised: March 14, 2023
Published: March 29, 2023

adsorption.[20] Cations larger than this optimum size either reduce the number of available adsorption sites by their larger occupancy or smaller cations compromise the accessibility due to their smaller size and require low temperatures and/or high pressures for CO_2 adsorption.[20] Water intercalation is controlled by the hydration energy of the cations;[18,31−33] however, for CO_2 intercalation, it has been argued that the interaction between the cation and the clay T−O−T (tetrahedral−octahedral−tetrahedral) structure plays a more important role.[11,29]

Hec is a synthetic and naturally occurring clay mineral that can be synthesized in a melt, resulting in large defect-free particles with a high charge homogeneity,[34] providing an excellent template for studying interactions with CO_2 without the interference of defects or impurities occurring in natural Hec. In previous works, we have shown that dried synthetic Ni-Hec readily adsorbs CO_2[5] and that this can be controlled by the layer charge magnitude,[19] where a lower layer charge results in a higher adsorption capacity and a lower pressure threshold for adsorption.[19] This CO_2 sorption capacity has been related to an ordered corrensite-like structure with alternating layers of hydrated Ni^{2+} cations and a condensed nickel hydroxide phase.[5,35] Here we study a synthetic Hec with only fluorine groups, whereas natural Hec has varying compositions of F^- and OH^- groups. Previous simulations[10] have shown that for increasing F^- over OH^- substitutions, the $CO_2/(CO_2 + H_2O)$ ratio increases and the total amount of $CO_2 + H_2O$ decreases.

Complete dehydration of smectite clays is challenging without venturing into a high-temperature region where the Hofmann−Klemen effect may occur.[36,37] Therefore, more systematic studies are required to investigate dehydrated clay minerals with different interlayer cations in response to CO_2. In the present work, we combine powder X-ray diffraction (PXRD) and gravimetric adsorption to study the swelling and uptake of CO_2 by dried Hec exchanged with the interlayer cations Li^+, Na^+, Cs^+, Ca^{2+}, and Ba^{2+} in order to reveal the driving mechanisms for swelling in response to CO_2. The experimental interpretations are fully supported by DFT calculations.

EXPERIMENTAL SECTION

Sample Preparation. Na-Hec with the stoichiometric composition of $Na(Mg_5Li)Si_8O_{20}F_4$ was prepared via melt synthesis according to a published procedure,[38] followed by annealing (6 weeks, 1045 °C) to improve charge homogeneity and phase purity.[34] To ensure the complete exchange for the different cations, Na-Hec was cation exchanged according to a published procedure[39] using an *n*-hexylamine solution, followed by treatment with a 2 M solution of LiOH, CsOH, $Ca(OH)_2$, and $Ba(OH)_2$. Ni-Hec was prepared by exchange with nickel acetate according to a published procedure.[35]

Thermogravimetric Analysis. The samples were characterized at NTNU with a Netzsch STA F3 449 Jupiter TGA measuring from 25 to 900 °C with a heating rate of 10 K/s under N_2 flow (20 mL/min purge, 10 mL/min protective)

X-ray Diffraction. X-ray diffraction patterns were collected at the XRD2 beamline at the Brazilian Synchrotron Light Laboratory, LNLS. A fixed wavelength of 1.305 Å was used, and the beam size was 0.3 mm × 0.3 mm. The scattering intensity was recorded by a Pilatus 300K area detector placed 114.8 mm from the sample. The 2D diffractograms were integrated using the software DAWN Science.[40] To control the temperature, an Oxford Cryojet5 was fixed at the sample position. The samples were injected into a high-pressure capillary cell, which was customized based on the design in ref 41. The cell was connected to a gas handling system with vacuum controlled by a HiCube turbomolecular pump and gas pressure from a bottle of CO_2 with a purity of 99.995%. The samples were heated in the capillaries to 150 °C under vacuum for drying, and the final drying was evaluated on the basis of the positions of the Bragg reflections. Samples were cooled to −20 °C, and if no peak movement was detected, then a pressure of 50 bar of CO_2 was applied while recording continuously.

Additional X-ray diffraction measurements were carried out at NTNU (Trondheim, Norway) using an in-house X-ray scattering instrument attached to a Xenocs stationary electron impact source with a copper anode, producing Kα radiation. The scattering intensity was recorded by a two-dimensional Dectris Pilatus3 R 200K detector. The samples were mounted in the same sample cell in contact with a temperature-regulated copper plate.[42] Temperature control was provided by Peltier elements, heat cartridges, and a circulation bath. The sample cell was connected to a gas handling system (Teledyne ISCO 260D) providing vacuum from a rotary vane pump (10^{-2} mbar) and pressurized CO_2 of 99.9992% purity.

Gravimetric Adsorption. CO_2 adsorption measurements were conducted with an IsoSORP gravimetric sorption analyzer from Rubotherm. Each sample was prepared by degassing at 120 ± 5 °C overnight under high vacuum and was considered to be dry when no more mass loss occurred. For each sample, two measurements were conducted with an equilibration time of 1 or 4 h at each pressure step from high vacuum to 35 bar. The temperature was measured with a Pt-100 temperature sensor placed directly underneath the sample crucible surrounded by a double-walled thermostat controlled by a CC-K6 circulating water bath from Huber. The temperature stability of the sample was within 22.5 ± 1 °C. The suspension balance has a resolution of 0.01 mg and a reproducibility of <0.002% rdg (~0.002 mg). The data for pressure, temperature, and sample weight were continuously recorded. The measured quantity is the excess adsorbed amount, which is obtained by correcting for the buoyancy of the skeletal volume of the sample material and the suspended metal parts (including the sample holder). The skeletal volume of the samples was determined by individual helium isotherms. The buoyancy of the suspended metal parts was obtained by a blank measurement with liquid CO_2. The density of helium and CO_2 for the given pressure and temperature conditions was obtained from the equation-of-state data provided by NIST.[43]

DFT Calculations: Methodology. Following the same methodological protocol described in our recent studies,[5,19,30] we perform first-principles calculations within the framework of density functional theory (DFT)[44,45] as implemented in the SIESTA package.[46] We considered a mesh cutoff of 400 Ry and a double-ζ plus polarization (DZP) basis set to represent the atomic charge in real space. The calculations were performed using the long-range van der Waals interactions implemented through the Berland and Hyldgaard[47] exchange-correlation functional. Also, we included the slab-dipole correction to minimize the spurious dipole effects emerging from the charge rearrangement observed in the system. Atomic positions of the interlayer species and molecules were established by minimizing the forces and energies until the residual forces were less than 0.01 eV/Å. The cohesive energy between clay layers is a measure of the energy needed to separate the layers from each other. To determine this energy within the DFT approach, we consider the interaction energy between the layers as a function of their separation distance, z. This interaction energy curve is calculated by comparing the total energy of the system at a given separation distance z perpendicular to the material's surface to a reference energy value obtained at a 100 Å separation layer distance (where the interaction between the layers is assumed to be minimal and may be neglected). This allows us to determine the energy required to separate the clay layers from each other, with those being at a given separation distance of z, and therefore compare the effect of each selected interlayer atom species on the cohesion. In addition to the cohesion energy, we also evaluated the adsorption energy of the CO_2 and H_2O molecules placed on top of the clay surface. To isolate the clay−molecule interactions from contributions in the adsorption energy coming from the spacial confinement, we consider a molecular model for the clay layer created

https://doi.org/10.1021/acs.langmuir.2c03093
Langmuir 2023, 39, 4895−4903

by adding a vacuum in the z direction perpendicular to the exposed surface. The vacuum given is sufficiently large, so the interaction between repeated surfaces toward the z axis decreases to the state where it may be ignored. Then, the molecular adsorption energy was evaluated by $E_{Ads} = E_{total} - (E_{clay} + E_{molecule})$, where E_{total} is the interacting system total energy and E_{clay} and $E_{molecule}$ are the total energies of the isolated clay with interlayer ions and gas molecules, respectively. The adsorption energy calculated in such a way shows the affinity between the clay surface and the foreign molecules (H_2O and CO_2), which may help to interpret, together with the cohesion energy, the role of interlayer atomic species in the interlayer physicochemical environment.

RESULTS AND DISCUSSION

X-ray Diffraction. The samples were cation exchanged by six different interlayer cations with different sizes and valencies and therefore different potentials to polarize the CO_2 molecules. In Figure 1, the dried state (heated to 150 °C for at least 1 h) and the final state at 50 bar of CO_2 at −20 °C (liquid CO_2) are shown for Hec with different cations. Their respective basal spacings between silicate layers are summarized in Table 1.

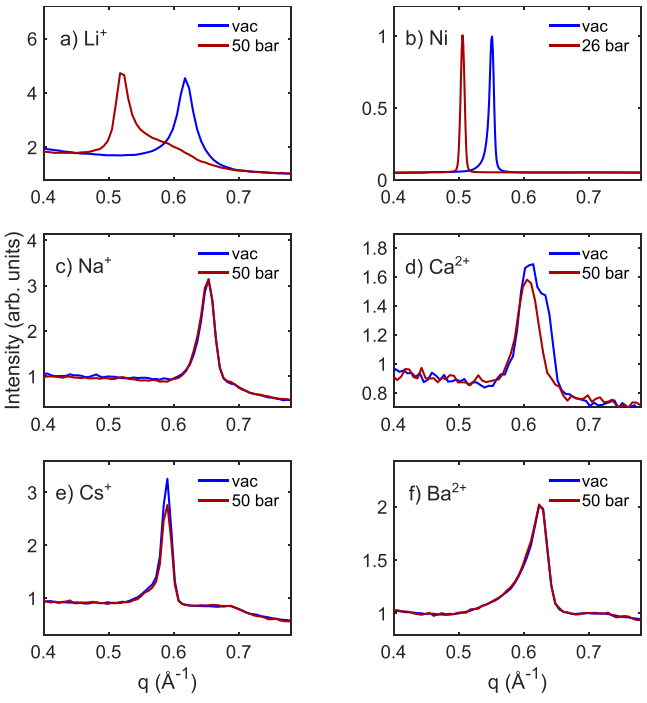

Figure 1. XRD pattern of the 001 peak in its dried state under vacuum and in response to 50 bar (26 bar for Ni-Hec) of CO_2 at −20 °C for the respective cations in Hec with (a) Li^+, (b) Ni, (c) Na^+, (d) Ca^{2+}, (e) Cs^+, and (f) Ba^{2+}. Ni-Hec was measured at SNBL BM01 at ESRF with the procedure given in ref 5. The remaining samples were measured at LNLS.

For the present work, Ni-Hec can be considered to be a reference, where the sample starts with a d_{002} of 11.4 Å in its dried state and swells to a final state of 12.3 Å. This swelling has previously been demonstrated in refs 5 and 19 to be due to the interaction with an ordered interstratified nickel hydroxide species.

The most evident result is the swelling for Li-Hec (Figure 1a), where it is initially observed at a basal spacing of 10.2 Å and swells to a final state of 12.2 Å. This is in full agreement with previous observations,[4] demonstrating that CO_2 is intercalated into Li-Hec. The asymmetric structure of the final Bragg reflection with a significant weight toward higher q values indicates that CO_2 is not fully intercalated in all interlayers under these experimental conditions.

Table 1. Basal Spacing of Hec with the Indicated Cations in the Dried and CO_2 Exposed States

cation	dried (Å)	CO_2 exposed (Å)
Li^+	10.2	12.2
Na^+	9.6	9.6
Cs^+	10.7	10.7
Ca^{2+}	10.0 and 10.3	10.3
Ba^{2+}	10.1	10.1

Na-Hec (Figure 1c), which is observed to have a basal spacing of 9.6 Å, in line with previous observations of dehydrated Na-Hec,[17] does not swell in response to CO_2, and there are no changes in the peak observed after CO_2 exposure, again confirming our previous reports.[30]

Upon drying of Ca-Hec, the Bragg reflection forms a double-peak structure with seemingly two phases (Figure 1d) at 10 and 10.3 Å, with a combined peak width significantly broader than that of the other ions investigated. After exposure to CO_2, the Bragg reflection forms a single symmetric peak at 10.3 Å. This suggests that Ca-Hec was not fully dehydrated and some residual water was left in the sample, producing two different environments with complete and incomplete dehydration. After CO_2 exposure, this was homogenized possibly through a pressure effect or by the diffusion of water in the CO_2 fluid phase. The absence of swelling from the initial state suggests that CO_2 is not intercalated to any significant extent in this case. Cs-Hec is initially found at a basal spacing of 10.7 Å (Figure 1e), in line with previous observations of a basal spacing of 10.8 Å for dried Cs-Hec.[48] This case also shows no significant response to CO_2. Finally, for Ba-Hec at an initial basal spacing of 10.1 Å (Figure 1f), no changes in the response to CO_2 are observed. This suggests that CO_2 is not intercalated into the clays with Na^+, Cs^+, Ca^{2+}, and Ba^{2+}, as intercalation chemistry dictates that the swelling must accommodate the real size of the CO_2 molecule (3.3 Å),[49] which neither of these do (e.g., for Cs-Hec 10.7−9.6 Å = 1 Å < 3.3 Å).

Li-Hec shows a response to CO_2 and remains in the swollen state even after reducing the CO_2 pressure to 1 bar (Figure 2), which is similar to what has previously been observed for this material.[4] Upon heating the sample, the basal spacing slowly shrinks with time and temperature, and after returning to ambient temperature, the Bragg reflection has returned to its initial dried position. This indicates some retention of CO_2 at temperatures below 0 °C and that CO_2 is completely released from the sample at approximately room temperature.

In the measurements described above, a full saturation of the sample in the CO_2 liquid phase is studied. When exposed to CO_2 gas at 23 °C, the evolution of the (001) Bragg reflection is as observed in Figure 3. There is slow growth as a function of the pressure of a peak at lower q values, which is the final product phase growing at the expense of the educt phase. Unlike Ni-Hec, which has previously been observed to have a clear pressure threshold before the full swollen state,[5] Li-Hec swells continuously in a nearly linear fashion over this pressure range. In accordance with the measurements at −20 °C (Figure 1a) at the final pressure, there is still intensity left in the educt phase, indicating a partial incorporation of CO_2 in the material. The gradual shift indicates that there is a random

https://doi.org/10.1021/acs.langmuir.2c03093
Langmuir 2023, 39, 4895−4903

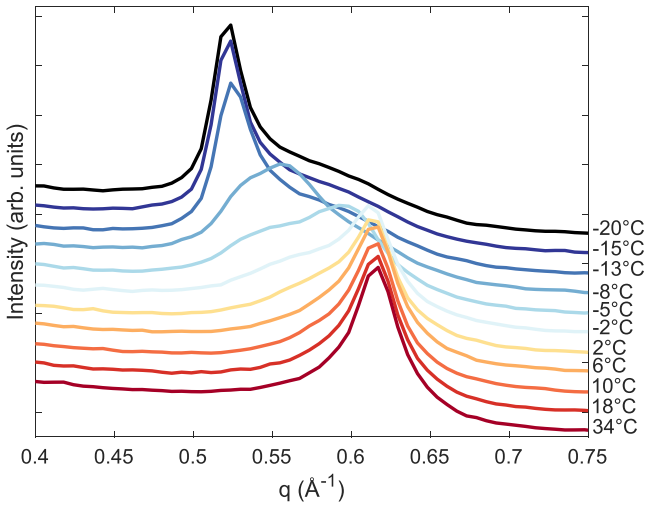

Figure 2. Powder X-ray diffraction of Li-Hec after reducing the pressure from 50 to 1 bar of CO_2 and subsequently heating the sample as indicated. The curves have been shifted vertically by an offset for clarity. Experiments were carried out at LNLS.

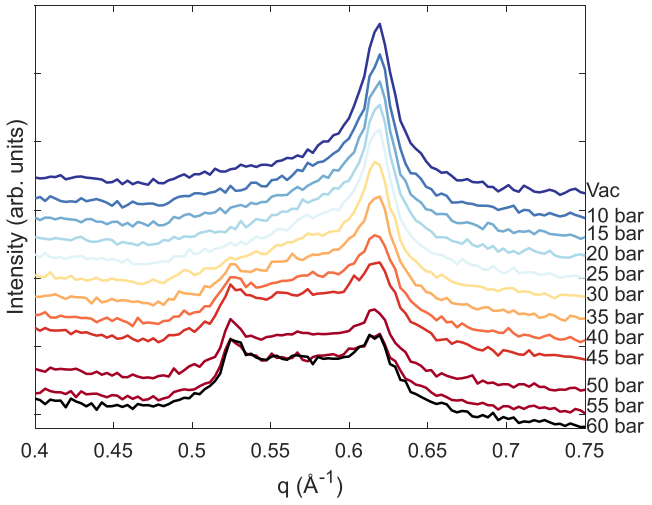

Figure 3. Powder X-ray diffraction of Li-Hec dried at 150 °C for 2.5 h and measured as a function of pressure for 1 h at each pressure step at 23 °C. The curves have been shifted vertically by an offset for clarity. Experiments were carried out at NTNU.

interstratification of CO_2 within the interlayers. The observations may suggest that the measurements are not at equilibrium or that there are sites in the interlayers where adsorption is hindered.

Gravimetric Adsorption Measurements. The gravimetric adsorption measurements were carried out only for Ni-Hec, Na-Hec, and Li-Hec and are shown in Figure 4. He isotherms were obtained over the same pressure range, giving densities of 2.35, 2.49, and 2.59 g/mL for Ni-Hec, Li-Hec, and Na-Hec, respectively. This is somewhat lower than the theoretical density of 2.8 g/mL for Na-Hec[17] and suggests that parts of the sample are inaccessible to He.

Similar to the PXRD measurements, there is no response in the gravimetric adsorption measurements for Na-Hec. The small hump around 30 bar for the Na-Hec measurement is within the error of the measurement. For Li-Hec, on the other hand, a linear response as a function of pressure is observed for the uptake, followed by hysteresis behavior upon reducing the

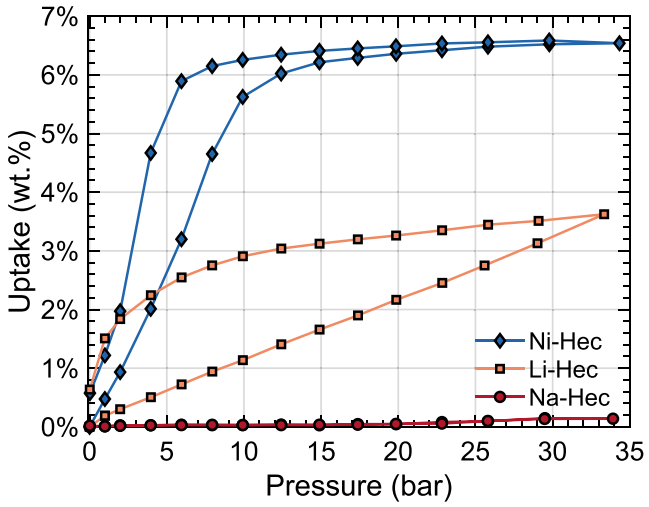

Figure 4. Gravimetric adsorption measurements of Na-Hec, Li-Hec, and Ni-Hec equilibrated at each pressure step for 4 h.

CO_2 pressure. Ni-Hec shows a response in accordance with slitlike pores opening up and accepting CO_2 homogeneously.[19] Li-Hec, on the other hand, follows a linear C-type adsorption isotherm.[50] Given the observations from XRD under the same conditions (Figure 3), this suggests that the swelling is not complete at 33 bar and that the increasing trend in uptake will hold at higher pressures. Upon desorption, the sample releases the CO_2, demonstrating that interaction with the clay mineral is reversible. Finally, at 35 bar an uptake of 6.5 wt. % (1.59 mmol/g) is observed for Ni-Hec, at 33 bar an uptake of 3.6 wt. % (0.85 mmol/g) is observed for Li-Hec, and for Na-Hec no uptake is observed. As previously demonstrated by the surface area measurements on Ni-Hec,[19] these clays provide a limited surface area; therefore, adsorption should largely occur in the interlayers, as is confirmed by the swelling behavior from the XRD measurements.

Li-Hec does swell and adsorb in response to CO_2. A possible explanation for this behavior is that Li-Hec may be a mixed-layer system where parts of the sample remain hydrated. Since Li^+ is a small interlayer cation with a small ionic radius, one would expect it to obtain a basal spacing similar to that of Na-Hec when it is dehydrated (9.6 as opposed to 10.2 Å). In this case, as much as 20% of the interlayer space may still contain water, which is supported by TGA (Figure 5). Li-Hec shows a much more sluggish dehydration behavior compared to Na-Hec. For Na-Hec, only a very limited residual water population has been observed by INS (inelastic neutron spectroscopy) to be left in the sample after dehydration to 145 °C.[30] Recent experiments on a Li-Hec from Corning[51] found that dried Li-Hec contains tightly bound water molecules that have a significantly higher adsorption energy, 225 kJ/mol compared to 31 kJ/mol for the more loosely bound water population in the sample. This is also highlighted in another work on Corning Li-Hec,[52] where water was observed by FTIR to desorb even above 200 °C. This water may then open up some of the layers sufficiently to allow for CO_2 adsorption to happen. This explains the linear adsorption isotherm, where the sites available for adsorption increase proportionally with the concentration of CO_2. The consequence of the open clay structure after the incorporation of CO_2 would be a higher diffusion rate for water or for Li^+ cations in the interlayers, eventually creating more sites for further CO_2 adsorption.

https://doi.org/10.1021/acs.langmuir.2c03093
Langmuir 2023, 39, 4895−4903

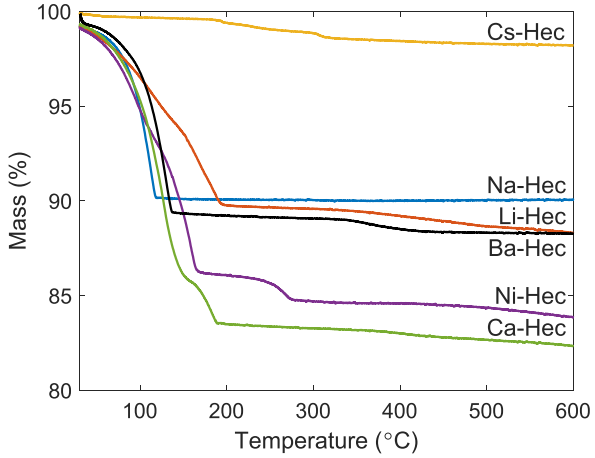

Figure 5. TGA of Li-Hec, Na-Hec, Cs-Hec, Ni-Hec, Ca-Hec, and Ba-Hec equilibrated at 43% RH.

Increased diffusion of interlayer cations with increased basal spacing has been observed by NMR spectroscopy in other clay systems.[11] The expansion of the interlayer space would be limited by the amount of water present in the system. This is supported by the observation of no clear single product phase in the PXRD measurements. As dehydration is hard to control for these systems, the sample in Figure 1 may be slightly more hydrated than the sample presented in Figure 3, as indicated by the clearer product phase. The present model where residual interlayer water assists the adsorption of CO_2 is in line with previous reports and interpretations of clay swelling in response to CO_2 with a hydration of between 0 and 1 WL.[12,23,27]

By additional heating of the Li-Hec sample to 280 °C, the gravimetric uptake is reduced significantly (Figure 6). At these

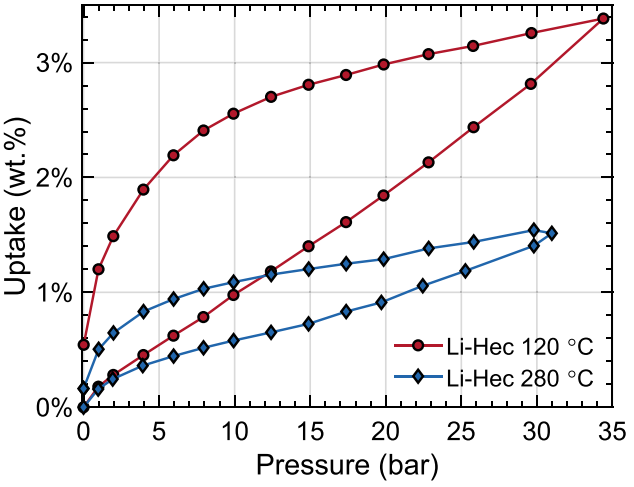

Figure 6. Gravimetric adsorption measurements of Li-Hec heated to 120 and 280 °C equilibrated at each pressure step for 1 h.

temperatures, the sample should be more dehydrated as indicated by the TGA (Figure 5). Still, there are residual adsorption sites, even after heating at high temperatures. At these temperatures, the Hofmann−Klemen effect will occur,[37] and some of the Li cations will migrate from the interlayer into the clay crystal structure.

For the remaining cations, the TGA shows sufficient dehydration behavior for Na-Hec and Ba-Hec at 150 °C (Figure 5), with the mass loss due to water prior to this temperature. For Cs-Hec, a low mass loss is observed due to its limited hydration because of the low hydration enthalpy.[53] For Ca-Hec, a second mass loss is observed at 180 °C, and similar to Li-Hec, sluggish dehydration behavior is found. The XRD data also suggest that the system had some water left. However, Ca-Hec does not swell in response to CO_2 under these experimental conditions. Repeated experiments on Ca-Hec have shown reproducible behavior in the response to CO_2. The absence of swelling for Ca-Hec can possibly be explained by the difference in solvation energies for CO_2 and H_2O by the two cations Li^+ and Ca^{2+}. As demonstrated by Criscenti and Cygan,[54] cations with a high solvation energy for water will partition preferentially into the H_2O phase. For cations with a solvation energy more similar to those of H_2O and CO_2, the cations may partition into the CO_2 fluid phase. Li^+ has a more comparable solvation energy in CO_2 or H_2O and therefore may be prone to allowing CO_2 to solvate the cation, whereas Ca^{2+} will prefer to interact with water molecules. Similar observations have been made on Mg-exchanged montmorillonite,[55] where it has been observed that predrying Mg-montmorillonite samples at different temperatures significantly affected the uptake of CO_2 and CH_4. In line with our conclusions, this was argued to be due to tightly bound residual water remaining in the interlayers of the smectite, thus opening them up for CO_2 adsorption.

The current observations confirm previous results for Na-Hec and other Na-smectites that the clay does not swell in response to CO_2 without the presence of water.[11,29,30] We can only speculate about the differences between the present work and refs 3, 4, and 6, but they may be attributed to the sample origin, charge, and phase purity as well as preparation methods including cation exchange (Li^+ to Na^+ for the commercial samples), drying procedures, and sample cells. Other studies have demonstrated that Cs^+-exchanged smectite can incorporate CO_2 when it is dehydrated under low vacuum at 50 °C[11] and at 450 °C under vacuum,[20] contrary to the present observations. At 50 °C, there may be some residual water left in the system; however, at 450 °C all water should be expelled. In ref 11, Wyoming MMT (SWy-2) is measured under supercritical conditions, and ref 20 demonstrates that the results still hold for the same clay mineral in the gaseous phase. We note that even at conditions corresponding to optimal uptake in ref 20 we do not observe swelling for Cs-Hec and Ba-Hec.

In this work, we have studied a high-quality synthetic clay mineral with respect to defects and impurities and with superior charge homogeneity.[34,56] This is a very important issue to consider when comparing the present work to other publications. In addition, we can consider a number of other possible explanations for the discrepancies. First, the smectites in the previously mentioned works[3,4,11,29] could have been insufficiently dehydrated. Second, clay−cation interactions, which have been suggested to be the dominant factor for CO_2 adsorption,[11] might be significantly different for our fluorinated Hec than for other smectites. For the works where MMT or other smectites have been studied, the clay−cation interaction is significantly different due to composition, charge density, charge homogeneity, and charge location within the layers. Such differences have been observed when examining SWy-2 and San Bernandino hectorite (SHCa-1), where

https://doi.org/10.1021/acs.langmuir.2c03093
Langmuir 2023, 39, 4895−4903

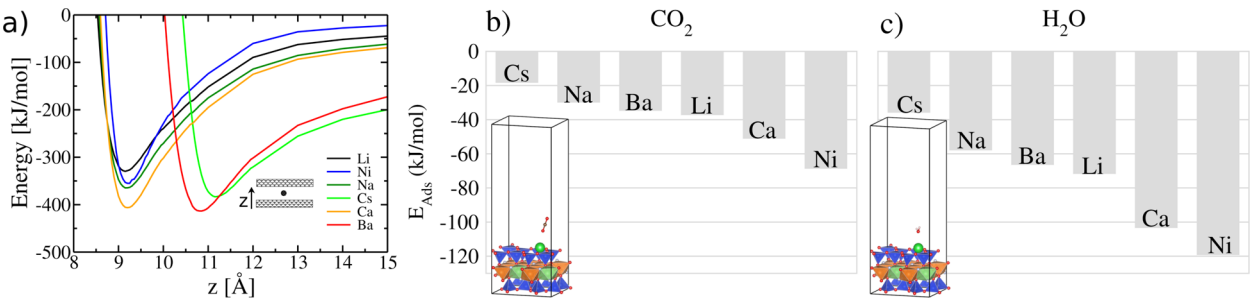

Figure 7. (a) Cohesion energy curves considering the different interlayer species. Adsorption energies of carbon dioxide (b) and water (c) molecules adsorbed above each interlayer atom in the clay material. The insets in panels (b) and (c) highlight the most stable configuration for the CO_2 and H_2O adsorption above the clay slab.

correlations with the influence of cation polarizability on the CO_2 adsorption were different between the two.[57] Comparing our results on fully fluorinated Hec with those of other natural Hec's, where there is a compositional difference due to a varying degree of F^- and OH^- substitutions, we would expect a higher CO_2 adsorption in the present case from simulations,[10] which is not the case. Third, for natural clays, side phases may significantly influence the uptake, for example, for Ni-Hec, where nickel hydroxide interstratified in the interlayer plays a dominant role in CO_2 adsorption.[5] In synthetic clay with high charge homogeneity, we have better control of the intercalation process and the history of the samples compared to natural systems. Finally, the layer charge for the current Hec is ∼40−80% higher than for the natural samples present in the other previously mentioned works,[11,20,29] which result in a higher cohesion energy holding the platelets together and thus hindering swelling/uptake in response to CO_2. Layer charge has been demonstrated for synthetic Ni-Hec to play a significant role in the adsorbed amount and pressure threshold for the swelling/adsorbing of CO_2.[19] In that case, a lower layer charge results in a lower pressure threshold, and it could be that the layer charge in this study is too high for the CO_2 to be able to penetrate the layers. The present clay with Cs^+ and Ba^{2+} has a higher charge and superior charge homogeneity compared to those of natural clays, which may explain why our synthetic case does not show CO_2 adsorption for these ions. This is an aspect that warrants further study.

DFT Calculations. We systematically evaluated the cohesion energy and the layer separation distance by considering each of the six investigated species in the clay interlayer space (Figure 7a). The cohesion energy gives information about how difficult it is to separate the clay layers. With Li as the interlayer cation, we observed that the separation process is expected to be more easily performed compared to the other ones. Otherwise, clays with Ca or Ba interlayer atoms are the ones that may display the most substantial glue effect. Interestingly, the layer separation distance of the dried phase is affected by the species with larger atomic radii, i.e., Ba and Cs. The minor differences in the atomic radii of Ca, Na, Li, and Ni species do not influence this property. We also determined the adsorption energy for both carbon dioxide (Figure 7b) and water (Figure 7c) molecules interacting with the most favorable site in the clay slab surrounded by a vacuum. Among the adsorption sites, both molecules display the lowest adsorption energy by interacting with the interlayer cation. We observed that these molecules have the highest affinity for the clays that have Ni, Ca, and Li as the interlayer ions. Additional evidence may explain the swelling in clays that have Li and Ni atoms within their composition. Although the interaction between H_2O, CO_2, and clays with Ca in the interlayer space is favorable, one should consider that this atom also contributes to the high cohesion energy, making it more difficult for the clay to swell. Also, the differences observed for water and carbon dioxide adsorption energies reveal the higher affinity of H_2O for the interlayer atom, to the detriment of CO_2. Indeed, the swelling phenomena occurring in Hec may involve a competition between the cohesive energy and the differences observed between the adsorption energies of the molecules in the interlayer space, where the interlayer species drives both effects.

CONCLUSIONS

We demonstrated that the selectivity for the intercalation of CO_2 into fluorohectorite clay depends on the interlayer cation. Dehydrated fluorohectorite with interlayer cations Na^+, Cs^+, Ca^{2+}, and Ba^{2+} did not swell or adsorb CO_2 when dried sufficiently. For Li-fluorohectorite, on the other hand, we observed swelling and adsorption, which we relate to tightly bound residual water that we were unable to remove without reaching the temperature regime where the Hoffman−Klemen effect would significantly alter the clay structure. The experimental results are supported by DFT calculations.

A full understanding of the details of the interactions between CO_2, residual water, and the interlayer cations, which may be obtained by spectroscopic measurements such as INS, IR, or Raman spectroscopy, would be helpful. In particular, this is needed to explain the interesting observations presented here for Li-Hec. To evaluate whether the discrepancies with the existing literature for the larger cations in this study are related to a cohesion energy that is too large due to the layer charge, further studies with Hec prepared at different layer charges will be conducted.

AUTHOR INFORMATION

Corresponding Authors

Kristoffer W. Bø Hunvik − *Department of Physics, Norwegian University of Science and Technology, N-7491 Trondheim, Norway;* orcid.org/0000-0002-2684-6464; Email: kristoffer.hunvik@ntnu.no

Jon Otto Fossum − *Department of Physics, Norwegian University of Science and Technology, N-7491 Trondheim, Norway;* orcid.org/0000-0002-8952-303X; Email: jon.fossum@ntnu.no

https://doi.org/10.1021/acs.langmuir.2c03093
Langmuir 2023, 39, 4895−4903

Authors

Konstanse Kvalem Seljelid − *Department of Physics, Norwegian University of Science and Technology, N-7491 Trondheim, Norway*

Dirk Wallacher − *Helmholtz-Zentrum-Berlin, 14109 Berlin, Germany*

Alexsandro Kirch − *Departamento de Física dos Materiais e Mecânica, Instituto de Física, Universidade de São Paulo, 05508-090 São Paulo, SP, Brazil*

Leide P. Cavalcanti − *Institute for Energy Technology (IFE), 2007 Kjeller, Norway;* Present Address: ISIS Neutron and Muon Source, Rutherford Appleton Laboratory, Chilton, Didcot OX11 0QX, United Kingdom

Patrick Loch − *Bavarian Polymer Institute and Department of Chemistry, University of Bayreuth, 95447 Bayreuth, Germany*

Paul Monceyron Røren − *Department of Physics, Norwegian University of Science and Technology, N-7491 Trondheim, Norway*

Paulo Henrique Michels-Brito − *Department of Physics, Norwegian University of Science and Technology, N-7491 Trondheim, Norway;* orcid.org/0000-0002-6320-1171

Roosevelt Droppa-Jr − *Universidade Federal do ABC (UFABC), Santo André, SP CEP 09210-580, Brazil*

Kenneth Dahl Knudsen − *Institute for Energy Technology (IFE), 2007 Kjeller, Norway; Department of Physics, Norwegian University of Science and Technology, N-7491 Trondheim, Norway*

Caetano Rodrigues Miranda − *Departamento de Física dos Materiais e Mecânica, Instituto de Física, Universidade de São Paulo, 05508-090 São Paulo, SP, Brazil*

Josef Breu − *Bavarian Polymer Institute and Department of Chemistry, University of Bayreuth, 95447 Bayreuth, Germany;* orcid.org/0000-0002-2547-3950

Complete contact information is available at: https://pubs.acs.org/10.1021/acs.langmuir.2c03093

Notes

The authors declare no competing financial interest.

■ ACKNOWLEDGMENTS

K.W.B.H., K.K.S., L.P.C., K.D.K., and J.O.F. were supported by the Research Council of Norway under the Frinatek Program (project number 250728). P.L. and J.B. were supported by the Deutsche Forschungsgemeinschaft (SFB 840). P.H.M.-B. acknowledges the support by NTNU. The authors gratefully acknowledge the Laboratorio Nacional de Luz Sincrotron (LNLS, Campinas, Brazil) for providing access to and support for the synchrotron facilities (XRD2-20170609 and XRD2-20180326). A.K. and C.R.M. gratefully acknowledge the Research Centre for Gas Innovation (RCGI), support from the Brazilian agencies FAPESP (2017/02317-2) and CNPq, and the resources supplied by the Center for Scientific Computing (NCC/GridUNESP) of Sao Paulo State University (UNESP).

■ REFERENCES

(1) Thomas, J.; Bohor, B. F. Surface area of montmorillonite from the dynamic sorption of nitrogen and carbon dioxide. *Clays and Clay Minerals* **1968**, *16*, 83−91.

(2) Fripiat, J.; Cruz, M.; Bohor, B.; Thomas, J. Interlamellar adsorption of carbon dioxide by smectites. *Clays and Clay Minerals* **1974**, *22*, 23−30.

(3) Hemmen, H.; Rolseth, E. G.; Fonseca, D. M.; Hansen, E. L.; Fossum, J. O.; Plivelic, T. S. X-ray studies of carbon dioxide intercalation in Na-fluorohectorite clay at near-ambient conditions. *Langmuir* **2012**, *28*, 1678−1682.

(4) Michels, L.; Fossum, J. O.; Rozynek, Z.; Hemmen, H.; Rustenberg, K.; Sobas, P. A.; Kalantzopoulos, G. N.; Knudsen, K. D.; Janek, M.; Plivelic, T. S.; et al. Intercalation and retention of carbon dioxide in a smectite clay promoted by interlayer cations. *Sci. Rep.* **2015**, *5*, 8775.

(5) Hunvik, K. W.; Loch, P.; Cavalcanti, L. P.; Seljelid, K. K.; Røren, P. M.; Rudic, S.; Knudsen, K. D.; Breu, J.; Bordallo, H. N.; Fossum, J. O. CO2 capture by nickel hydroxide interstratified in the nanolayered space of a synthetic clay mineral. *J. Phys. Chem. C* **2020**, *124*, 26222−26231.

(6) Cavalcanti, L. P.; Kalantzopoulos, G. N.; Eckert, J.; Knudsen, K. D.; Fossum, J. O. A nano-silicate material with exceptional capacity for CO 2 capture and storage at room temperature. *Sci. Rep.* **2018**, *8*, 11827.

(7) Hwang, J.; Joss, L.; Pini, R. Measuring and modelling supercritical adsorption of CO2 and CH4 on montmorillonite source clay. *Microporous Mesoporous Mater.* **2019**, *273*, 107−121.

(8) Giesting, P.; Guggenheim, S.; Van Groos, A. F. K.; Busch, A. Interaction of carbon dioxide with Na-exchanged montmorillonite at pressures to 640 bar: Implications for CO2 sequestration. *International Journal of Greenhouse Gas Control* **2012**, *8*, 73−81.

(9) Loring, J. S.; Schaef, H. T.; Thompson, C. J.; Turcu, R. V.; Miller, Q. R.; Chen, J.; Hu, J.; Hoyt, D. W.; Martin, P. F.; Ilton, E. S.; et al. Clay hydration/dehydration in dry to water-saturated supercritical CO2: implications for caprock integrity. *Energy Procedia* **2013**, *37*, 5443−5448.

(10) Loganathan, N.; Yazaydin, A. O.; Kirkpatrick, R. J.; Bowers, G. M. Tuning the Hydrophobicity of Layer-Structure Silicates To Promote Adsorption of Nonaqueous Fluids: Effects of F−for OH− Substitution on CO2 Partitioning into Smectite Interlayers. *J. Phys. Chem. C* **2019**, *123*, 4848−4855.

(11) Schaef, H. T.; Loganathan, N.; Bowers, G. M.; Kirkpatrick, R. J.; Yazaydin, A. O.; Burton, S. D.; Hoyt, D. W.; Thanthiriwatte, K. S.; Dixon, D. A.; McGrail, B. P.; et al. Tipping point for expansion of layered aluminosilicates in weakly polar solvents: supercritical CO2. *ACS Appl. Mater. Interfaces* **2017**, *9*, 36783−36791.

(12) Rother, G.; Ilton, E. S.; Wallacher, D.; Hauβ, T.; Schaef, H. T.; Qafoku, O.; Rosso, K. M.; Felmy, A. R.; Krukowski, E. G.; Stack, A. G.; et al. CO2 sorption to subsingle hydration layer montmorillonite clay studied by excess sorption and neutron diffraction measurements. *Environ. Sci. Technol.* **2013**, *47*, 205−211.

(13) Schaef, H. T.; Davidson, C. L.; Owen, A. T.; Miller, Q. R.; Loring, J. S.; Thompson, C. J.; Bacon, D. H.; Glezakou, V. A.; McGrail, B. P. CO2 utilization and storage in shale gas reservoirs: experimental results and economic impacts. *Energy Procedia* **2014**, *63*, 7844−7851.

(14) Busch, A.; Alles, S.; Gensterblum, Y.; Prinz, D.; Dewhurst, D. N.; Raven, M. D.; Stanjek, H.; Krooss, B. M. Carbon dioxide storage potential of shales. *International journal of greenhouse gas control* **2008**, *2*, 297−308.

(15) Busch, A.; Bertier, P.; Gensterblum, Y.; Rother, G.; Spiers, C.; Zhang, M.; Wentinck, H. M. On sorption and swelling of CO 2 in clays. *Geomechanics and Geophysics for Geo-energy and Geo-resources* **2016**, *2*, 111−130.

(16) Bergaya, F.; Lagaly, G. *Handbook of Clay Science*; Newnes, 2013; pp 1−18.

(17) Kalo, H.; Milius, W.; Breu, J. Single crystal structure refinement of one-and two-layer hydrates of sodium fluorohectorite. *Rsc Advances* **2012**, *2*, 8452−8459.

(18) Da Silva, G.; Fossum, J.; DiMasi, E.; Måløy, K. Hydration transitions in a nanolayered synthetic silicate: A synchrotron x-ray scattering study. *Phys. Rev. B* **2003**, *67*, 094114.

(19) Hunvik, K. W. B.; Loch, P.; Wallacher, D.; Leide, C.; Riess, M.; Grätz, S.; Yokaichiya, F.; Knudsen, K. D.; Breu, J.; Fossum, J. O. CO_2

Adsorption Enhanced by Tuning the Layer Charge in a Clay Mineral. *Langmuir* **2021**, *37*, 14491−14499.
(20) Mendel, N.; Sîretanu, D.; Sîretanu, I.; Brilman, D. W.; Mugele, F. Interlayer Cation-Controlled Adsorption of Carbon Dioxide in Anhydrous Montmorillonite Clay. *J. Phys. Chem. C* **2021**, *125*, 27159−27169.
(21) Kadoura, A.; Narayanan Nair, A. K.; Sun, S. Molecular simulation study of montmorillonite in contact with variably wet supercritical carbon dioxide. *J. Phys. Chem. C* **2017**, *121*, 6199−6208.
(22) Loring, J. S.; Schaef, H. T.; Turcu, R. V.; Thompson, C. J.; Miller, Q. R.; Martin, P. F.; Hu, J.; Hoyt, D. W.; Qafoku, O.; Ilton, E. S.; et al. In situ molecular spectroscopic evidence for CO2 intercalation into montmorillonite in supercritical carbon dioxide. *Langmuir* **2012**, *28*, 7125−7128.
(23) Loring, J. S.; Ilton, E. S.; Chen, J.; Thompson, C. J.; Martin, P. F.; Bénézeth, P.; Rosso, K. M.; Felmy, A. R.; Schaef, H. T. In situ study of CO2 and H2O partitioning between Na−montmorillonite and variably wet supercritical carbon dioxide. *Langmuir* **2014**, *30*, 6120−6128.
(24) Rao, Q.; Leng, Y. Molecular understanding of CO2 and H2O in a montmorillonite clay interlayer under CO2 geological sequestration conditions. *J. Phys. Chem. C* **2016**, *120*, 2642−2654.
(25) Lee, M.-S.; McGrail, B. P.; Glezakou, V.-A. Microstructural response of variably hydrated Ca-rich montmorillonite to supercritical CO2. *Environ. Sci. Technol.* **2014**, *48*, 8612−8619.
(26) Schaef, H. T.; Ilton, E. S.; Qafoku, O.; Martin, P. F.; Felmy, A. R.; Rosso, K. M. In situ XRD study of Ca2+ saturated montmorillonite (STX-1) exposed to anhydrous and wet supercritical carbon dioxide. *International Journal of Greenhouse Gas Control* **2012**, *6*, 220−229.
(27) Schaef, H. T.; Loring, J. S.; Glezakou, V.-A.; Miller, Q. R.; Chen, J.; Owen, A. T.; Lee, M.-S.; Ilton, E. S.; Felmy, A. R.; McGrail, B. P.; et al. Competitive sorption of CO2 and H2O in 2:1 layer phyllosilicates. *Geochim. Cosmochim. Acta* **2015**, *161*, 248−257.
(28) Myshakin, E. M.; Saidi, W. A.; Romanov, V. N.; Cygan, R. T.; Jordan, K. D. Molecular dynamics simulations of carbon dioxide intercalation in hydrated Na-montmorillonite. *J. Phys. Chem. C* **2013**, *117*, 11028−11039.
(29) Loganathan, N.; Bowers, G. M.; Yazaydin, A. O.; Schaef, H. T.; Loring, J. S.; Kalinichev, A. G.; Kirkpatrick, R. J. Clay swelling in dry supercritical carbon dioxide: effects of interlayer cations on the structure, dynamics, and energetics of CO2 intercalation probed by XRD, NMR, and GCMD simulations. *J. Phys. Chem. C* **2018**, *122*, 4391−4402.
(30) Hunvik, K. W. B.; Lima, R. J. d. S.; Kirch, A.; Loch, P.; Monceyron Røren, P.; Hoffmann Petersen, M.; Rudic, S.; Garcia Sakai, V.; Knudsen, K. D.; Rodrigues Miranda, C.; et al. Influence of CO2 on Nanoconfined Water in a Clay Mineral. *J. Phys. Chem. C* **2022**, *126*, 17243−17254.
(31) Loganathan, N.; Yazaydin, A. O.; Bowers, G. M.; Kalinichev, A. G.; Kirkpatrick, R. J. Structure, energetics, and dynamics of Cs+ and H2O in hectorite: Molecular dynamics simulations with an unconstrained substrate surface. *J. Phys. Chem. C* **2016**, *120*, 10298−10310.
(32) Loganathan, N.; Yazaydin, A. O.; Bowers, G. M.; Kalinichev, A. G.; Kirkpatrick, R. J. Cation and Water Structure, Dynamics, and Energetics in Smectite Clays: A Molecular Dynamics Study of Ca−Hectorite. *J. Phys. Chem. C* **2016**, *120*, 12429−12439.
(33) Lindholm, J.; Boily, J.-F.; Holmboe, M. Deconvolution of Smectite Hydration Isotherms. *ACS Earth and Space Chemistry* **2019**, *3*, 2490−2498.
(34) Stöter, M.; Kunz, D. A.; Schmidt, M.; Hirsemann, D.; Kalo, H.; Putz, B.; Senker, J.; Breu, J. Nanoplatelets of sodium hectorite showing aspect ratios of 20 000 and superior purity. *Langmuir* **2013**, *29*, 1280−1285.
(35) Loch, P.; Hunvik, K. W.; Puchtler, F.; Weiss, S.; Seljelid, K. K.; Røren, P. M.; Rudic, S.; Knudsen, K. D.; Raaen, S.; Bordallo, H. N.; et al. Spontaneous Formation of an Ordered Interstratification upon Ni-exchange. *Appl. Clay Sci.* **2020**, *198*, 105831−105840.
(36) Hofmann, U.; Klemen, R. Verlust der austauschfähigkeit von lithiumionen an bentonit durch erhitzung. *Zeitschrift für anorganische Chemie* **1950**, *262*, 95−99.
(37) Komadel, P.; Madejová, J.; Bujdák, J. Preparation and properties of reduced-charge smectites—a review. *Clays and Clay Minerals* **2005**, *53*, 313−334.
(38) Daab, M.; Eichstaedt, N. J.; Habel, C.; Rosenfeldt, S.; Kalo, H.; Schießling, H.; Förster, S.; Breu, J. Onset of Osmotic Swelling in Highly Charged Clay Minerals. *Langmuir* **2018**, *34*, 8215−8222.
(39) Hiebl, C.; Loch, P.; Brinek, M.; Gombotz, M.; Gadermaier, B.; Heitjans, P.; Breu, J.; Wilkening, H. M. R. Rapid Low-Dimensional Li + Ion Hopping Processes in Synthetic Hectorite-Type Li0. 5 [Mg2. 5Li0. 5] Si4O10F2. *Chem. Mater.* **2020**, *32*, 7445−7457.
(40) Filik, J.; Ashton, A.; Chang, P.; Chater, P.; Day, S.; Drakopoulos, M.; Gerring, M.; Hart, M.; Magdysyuk, O.; Michalik, S.; et al. Processing two-dimensional X-ray diffraction and small-angle scattering data in DAWN 2. *Journal of applied crystallography* **2017**, *50*, 959−966.
(41) Jensen, T. R.; Nielsen, T. K.; Filinchuk, Y.; Jørgensen, J.-E.; Cerenius, Y.; Gray, E. M.; Webb, C. J. Versatile in situ powder X-ray diffraction cells for solid−gas investigations. *Journal of applied crystallography* **2010**, *43*, 1456−1463.
(42) Røren, P. M.; Hunvik, K. W. B.; Josvanger, V.; Buseth, O. T.; Fossum, J. O. Controlled sample environment for studying solid−gas interactions by *in situ* powder X-ray diffraction. *J. Appl. Crystallogr.* **2021**, *54*, 371−375.
(43) Lemmon, E. W.; McLinden, M. O.; Friend, D. G. Thermophysical Properties of Fluid Systems; *NIST Standard Reference Database Number 69*; retrieved June 22, 2020.
(44) Hohenberg, P.; Kohn, W. Inhomogeneous electron gas. *Physical review* **1964**, *136*, B864.
(45) Kohn, W.; Sham, L. J. Self-consistent equations including exchange and correlation effects. *Physical review* **1965**, *140*, A1133.
(46) Soler, J. M.; Artacho, E.; Gale, J. D.; García, A.; Junquera, J.; Ordejón, P.; Sánchez-Portal, D. The SIESTA method for ab initio order-N materials simulation. *J. Phys.: Condens. Matter* **2002**, *14*, 2745.
(47) Berland, K.; Hyldgaard, P. Exchange functional that tests the robustness of the plasmon description of the van der Waals density functional. *Phys. Rev. B* **2014**, *89*, 035412.
(48) Seidl, W.; Breu, J. Single crystal structure refinement of tetramethylammonium-hectorite. *Zeitschrift für Kristallographie-Crystalline Materials* **2005**, *220*, 169−176.
(49) Lewis, J. Gas Separation Membranes: Polymeric and Inorganic. *Chemical Engineering Education* **2018**, *52*, 223.
(50) Limousin, G.; Gaudet, J.-P.; Charlet, L.; Szenknect, S.; Barthes, V.; Krimissa, M. Sorption isotherms: A review on physical bases, modeling and measurement. *Applied geochemistry* **2007**, *22*, 249−275.
(51) Larsen, S. R.; Michels, L.; dos Santos, É. C.; Berg, M. C.; Gates, W. P.; Aldridge, L. P.; Seydel, T.; Ollivier, J.; Telling, M. T.; Fossum, J.-O.; et al. Physicochemical characterisation of fluorohectorite: Water dynamics and nanocarrier properties. *Microporous Mesoporous Mater.* **2020**, *306*, 110512.
(52) dos Santos, E.; Gates, W.; Michels, L.; Juranyi, F.; Mikkelsen, A.; da Silva, G.; Fossum, J.; Bordallo, H. The pH influence on the intercalation of the bioactive agent ciprofloxacin in fluorohectorite. *Appl. Clay Sci.* **2018**, *166*, 288−298.
(53) Möller, M. W.; Handge, U. A.; Kunz, D. A.; Lunkenbein, T.; Altstädt, V.; Breu, J. Tailoring shear-stiff, mica-like nanoplatelets. *ACS Nano* **2010**, *4*, 717−724.
(54) Criscenti, L. J.; Cygan, R. T. Molecular simulations of carbon dioxide and water: cation solvation. *Environ. Sci. Technol.* **2013**, *47*, 87−94.
(55) Grekov, D. I.; Suzuki-Muresan, T.; Kalinichev, A. G.; Pré, P.; Grambow, B. Thermodynamic data of adsorption reveal the entry of CH4 and CO2 in smectite clay interlayer. *Phys. Chem. Chem. Phys.* **2020**, *22*, 16727.
(56) Rosenfeldt, S.; Stoter, M.; Schlenk, M.; Martin, T.; Albuquerque, R. Q.; Forster, S.; Breu, J. In-depth insights into the

https://doi.org/10.1021/acs.langmuir.2c03093
Langmuir 2023, 39, 4895−4903

key steps of delamination of charged 2D nanomaterials. *Langmuir* **2016**, *32*, 10582−10588.
(57) Cunniff, S. S.; Schaef, H. T.; Burton, S. D.; Walter, E. D.; Hoyt, D. W.; Loring, J. S.; Bowers, G. M. Interlayer Cation Polarizability Affects Supercritical Carbon Dioxide Adsorption by Swelling Clays. *Langmuir* **2022**, *38*, 15540−15551.

https://doi.org/10.1021/acs.langmuir.2c03093
Langmuir 2023, 39, 4895−4903